We are IntechOpen,
the world's leading publisher of
Open Access books
Built by scientists, for scientists

6,900
Open access books available

186,000
International authors and editors

200M
Downloads

Our authors are among the

154
Countries delivered to

TOP 1%
most cited scientists

12.2%
Contributors from top 500 universities

CLARIVATE ANALYTICS
BOOK CITATION INDEX
INDEXED

WEB OF SCIENCE™

Selection of our books indexed in the Book Citation Index
in Web of Science™ Core Collection (BKCI)

Interested in publishing with us?
Contact book.department@intechopen.com

Numbers displayed above are based on latest data collected.
For more information visit www.intechopen.com

Influence of Surface Treatment on the Conversion Efficiency of Thin-Film a-Si:H Solar Cells on a Stainless Steel Substrate

Wen-Cheng Ke and Shuo-Jen Lee

Additional information is available at the end of the chapter

1. Introduction

Over the past decade, hydrogenated amorphous silicon (a-Si:H) thin-film solar cells have emerged as a viable substitute for solid-state silicon solar cells. The a-Si:H thin-film solar cells gained importance primarily due to their low production cost, and eco-friendly nature [1-3]. However, these cells have the inherent disadvantage of using glass as a substrate material, which makes the cells unsuitable for use in a round shaped product, are heavy and have a high material cost. Replacing the glass substrate with a stainless steel (SS) substrate makes it possible to fabricate lightweight, thin, and low-cost a-Si:H thin-film solar cells using roll-to-roll mass production [4,5]. However, the surface morphology of a SS substrate is of poorer quality than that of the glass substrate. For the past several years flexible solar cells fabricated on a stainless steel substrate are being widely used for the building of integrated photovoltaics (BIPVs). Stainless steel has many advantages, such as low cost, high extension, ease of preparing etc. Thus it was commonly believed that the wide application of BIPVs especially rooftop applications, would be the biggest market for flexible PV technology [1-4], especially since these flexible products are very light, and quick and easy to install. Indeed, BIPV products did see a rapid growth in recent years, with more companies going into production. However, the main challenge of BIPVs remains. The question of how to improve the conversion efficiency has not been resolved.

The main limitation of thin-film solar cell efficiency is the long absorption length of the long wavelength photons and the thinness of the absorbing layer. The absorption length of a-Si:H with a bandgap of 1.6 eV, for the red and infrared solar photons, exceeds 1 μm and 100 μm, respectively [6,7]. In addition, for a-Si:H the hole diffusion length is 300–400 nm, which lim-

its the solar cell absorber layer thickness to less than the hole diffusion length [8]. This makes it exceedingly difficult to harvest these photons since the absorber thickness of a p-i-n single junction solar cell is limited to only a few hundred nanometers for efficient carrier collection. Thus, increasing the light absorption is essential for the design of thin-film solar cells [9–12]. Maximum light absorption is achieved using several different techniques including back-reflector or light trapping configurations. Enhanced light-trapping in thin-film solar cells is typically achieved by a textured oxide layer on the metal back-reflector that scatters light within the absorbing layer and increases the optical path-length of the solar photons. In our latest research [13,14], we fabricated a textured SS substrate using the photolithography method to increase the light scattering. Unfortunately, the electrical properties of a-Si:H thin-film solar cells deposited on these micro-size textured SS substrates are not stable. There are many deep etching pits on the textured SS substrate surface, resulting in a non-uniform thickness of the a-Si:H thin-film deposited on the whole textured SS substrate surface. This non-uniform coverage of the a-si:H layer on the textured 304 SS usually fails to perform its function in the thin-film solar cells. Thus, the surface morphology of the SS substrate plays an important role in achieving the stable electrical properties of the a-Si:H thin-film solar cells.

In addition, it is well known that defects in thin-film solar cells increase the series resistance (Rs) and decrease the shunt resistance (Rsh), resulting in a decreased open voltage (V_{OC}) and short current density (J_{sc}) of the thin-film solar cells. Although a number of investigations were carried out to study the properties of the defects in crystalline Si solar cells [15,16], a detailed understanding of a-Si:H thin-film solar cells is still lacking. Iron (Fe), one of the most common impurities in crystalline Si solar cell materials, has a detrimental effect on the minority carrier lifetime due to the defect states introduced by Fe and its complexes with acceptors in the band gap of silicon [17,18]. It has been suggested that diffusion of detrimental elements, such as Fe from stainless steel, into the a-Si:H layer as a result of high temperatures during the a-Si:H processing, deteriorate the cell's efficiency. In this study, a thick (exceeding 2-μm) metal Mo buffer layer is used to reduce the diffusion of Fe impurities from the 304 SS substrate. The influence of the Fe impurities on the cell's performance was investigated carefully. Additionally, Electro-polishing (EP) and Electrical chemical mechanical polish (ECMP) processes have been used to improve the surface roughness of the stainless steels, and make them more suitable as a substrate for a-Si:H thin-film solar cells. The EP and ECMP dissolve metal ions electrochemically by applying an anodic potential on the SS substrate surface in an aqueous electrolyte [19-22]. It should be noted that the ECMP also removes a passivation layer by the mechanical abrasion of the polishing pad and the abrasives in the electrolyte. After the EP or ECMP process is finished, the SS substrate surface forms a hard and dense Cr-rich passivation layer which is expected to block the diffusion of metal impurities from the SS substrate into a-Si:H layer. We carefully investigated the conversion efficiency of a-Si:H thin-film solar cells based on the surface morphology and impurity diffusion of 304 SS substrate treated by the EP and ECMP processes.

2. Surface-treated process of 304 stainless steel substrate

2.1. Electro-polishing process

In the 1980's, most of the research reports indicated that the EP process of the stainless steel substrate began by forming a viscous layer on the substrate surface resulting in the formation of a passivation layer. Generally, the high spike has a higher dissolve velocity in the viscous layer providing the initial polish of the stainless steel substrate. Once the EP process has ran for a long enough time, a dense passivation layer or metal-rich oxidation layer will form at the bottom of the viscous layer on the surface of the substrate resulting in a smooth surface. The viscous layer formation mechanism in the EP pricess is a key parameter for achieving a smooth surface stainless steel substrate. There are some conditions, such as solution convection, ion diffusion, electrical current distribution and electron migration will determine the EP results. Thus, the applying voltage, current, gap between the anode and cathode, reaction time, cathode design must be controlled carefully. The schematic diagrams of the EP system are shown in Fig. 1. In this study, the 304 stainless steel substrate with thickness of 1 mm was clipped by the anode clamp. The stainless steel net was used as the cathode plate. The important parameter lists of the EP process are listed in Table 1. After the EP process, the mirror-like surface of the 304 stainless steel substrate can be achieved (Fig. 2).
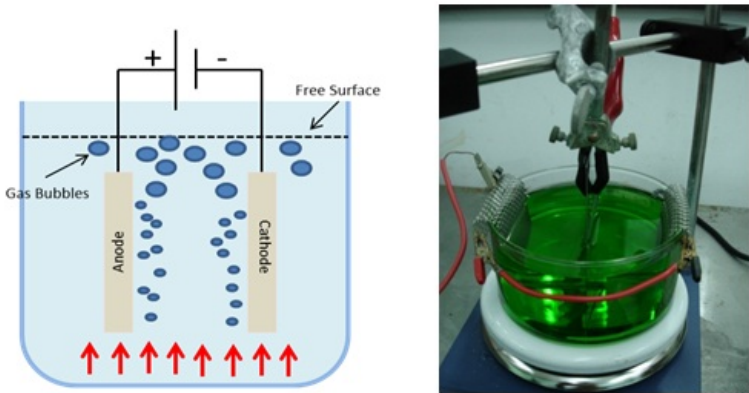

Figure 1. The schematic diagram of the EP system.

EP process	Parameters
Reaction time	1 min
Voltage/current	3.3 V/4.5 A
Temperature	70°C
Electrolyte	$C_3H_5(OH)_3$:H_2O = 1:1 H_2SO_4:H_3PO_4 = 0.29

**Table 1.** The key parameters of the EP process.

Figure 2. The image of the mirror-like 304 stainless steel substrate after the EP process.

2.2. Electrical chemical mechanical polish process

The schematic diagrams of the ECMP system are shown in Fig. 3 and Fig. 4. The ECMP process consists of both electrochemical and mechanical polishing mechanisms, electrolysis and physical polishing, to repair the irregular surface morphology of the 304 SS substrate. In addition, the mechanical friction between the polishing pad and the 304 SS substrate induces an interactive force that removes the surface oxidation layer or passivation layer that forms during the electrolysis process. It should be noted that no peeling force is generated during the ECMP process, and thus there is no need to consider any mechanical deformation of the substrate. The ECMP process base on the fundamental electrochemical reaction terms as following:

Anode chemical reaction:

$$M^+ + OH^- \rightarrow \grave{e}MOH \tag{1}$$
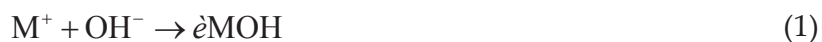
Cathode chemical reaction:

$$2H^+ \rightarrow \grave{e}H_2 \tag{2}$$

The important parameters of ECMP process are described in the list below.

1. The 304 stainless steel substrate was first cleaned by acetone and DI water in order to remove the oil and particle contaminant.

2. Polishing solution with 50g of 1μm Al_2O_3 powder in 0.5 L DI water.

3. Electrolyte solution ($NaNO_3$) with concentration of 3 wt%.

The other important parameter lists of the ECMP process are listed in Table 2. In Fig. 5, the mirror-like surface of the 304 stainless steel substrate can be achieved after the ECMP process.
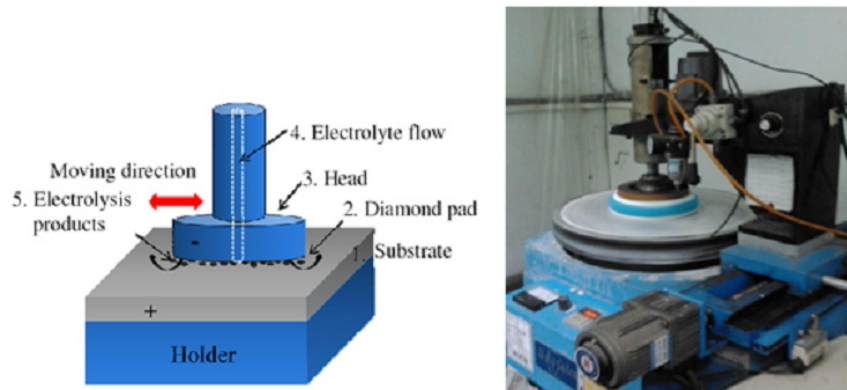

Figure 3. The schematic diagram of the ECMP system.

3. Effect of Mo blocking layer on the conversion efficiency of a-Si:H solar cells

3.1. Experimental details

In this study, a series of p-i-n solar cells were deposited on a 304 SS substrate by high frequency plasma enhanced chemical vapor deposition (HF-PECVD), in an ultrahigh-vacuum, single-chamber, load-locked system at a constant temperature of 200 °C. The

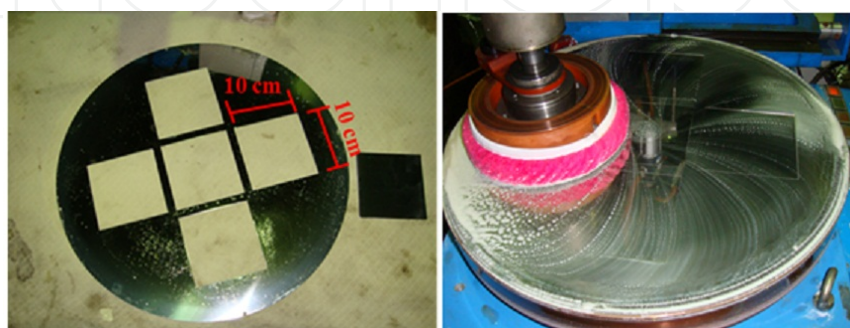**Figure 4.** The sample holder and polishing process image of the ECMP system.

ECMP process	Parameters
Polishing time	20 min
Voltage/current	7 V/1 A
Rotation speed (anode holder)	30 rpm
Rotati speed (Cathode head)	40 rpm

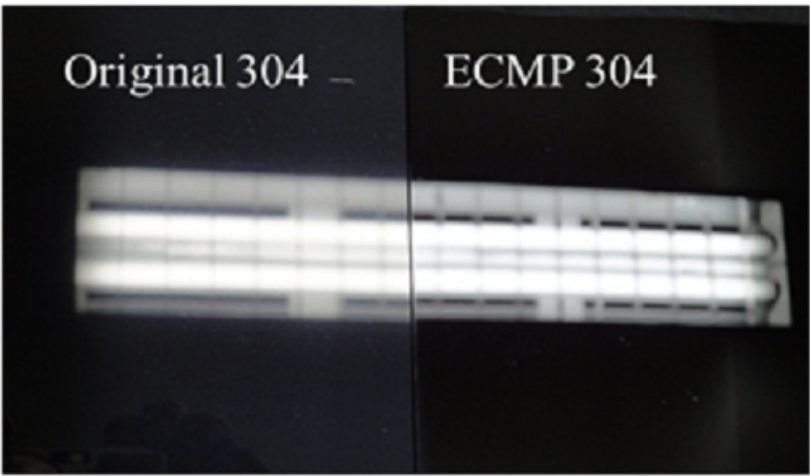**Table 2.** The key parameters of the ECMP process.

Figure 5. The image of the mirror-like 304 stainless steel substrate after the ECMP process.

thickness of the p-i-n layers in the solar cell structure were 10, 300, and 20 nm respectively. In order to avoid diffusion by Fe impurities diffusing from the 304 SS substrate into Si solar cells and to study its influence on cell efficiency (see Fig. 6), we designed a series of cell structures including Ag/AZO/n-i-p/SS, Ag/AZO/n-i-p/Ag/SS, Ag/AZO/n-i-p/Ag/0.5-μm-thick Mo/SS, and Ag/AZO/n-i-p/Ag/2.0-μm-thick Mo/SS. It was crucial that no alumina-zinc-oxide (AZO) layer would grow between the 304 SS substrate and the a-Si:H cell so that we could clearly observe the change in cell performance as a result of preventing the diffusion of Fe impurities. All metal and transparent conductive oxide layers in the structure of the cells were deposited by radio frequency (RF) magnetron sputtering. The thickness of the back reflection metal Ag and AZO layers were 200 and 150 nm, respectively. It should be noted that the metal Mo layers, 0.5-μm-thick and 2-μm-thick were deposited on a 304 SS substrate by adjusting the sputtering power to 100 W and 500 W, respectively. The Ar gas flow rate was kept at 30 sccm, and the deposition time was kept at 30 min. In general, high sputtering power can achieve a higher metal deposition rate. The solar cell performance was determined using a calibrated AM 1.5G solar simulator under illumination, and operating at a light intensity of 100 mW/cm^2. The current-voltage (I-V) curves were obtained using the Keithley 2400 SourceMeter. The optical properties of the raw 304 SS substrate and the 304 SS

substrate coated with Ag and Ag/Mo films were measured by a UV-visible(Vis)-near IR (NIR) spectrophotometer (Perkin Elmer Lambda 750s) in the 400-700 nm wavelength range. The samples were measured with a secondary ion mass spectroscope (SIMS) in order to analyze the diffusion of Fe impurities from the 304 SS substrate into the cell structure.
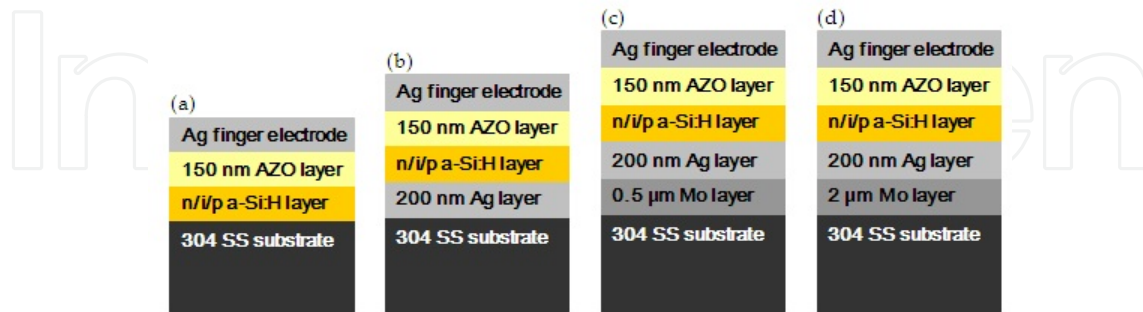

Figure 6. Cross-sectional schematic diagrams for the samples of this study.

3.2. Morphological properties

Figure 7 shows the SEM images of a metal Mo buffer layer with varying thickness on a 304 SS substrate. In Fig. 7(a), the small size of the Mo grains and the grain direction are a random distribution when the sputtering power is low (i.e. low deposition rate = 0.28 nm/sec). In contrast, the long ridge and the ordered arrangement of the large Mo grains was achieved by a high-power sputtering process (i.e. deposition rate = 1.11 nm/sec). In addition, the grain boundary decreased due to the increased merging of the Mo grains into the high-power sputtered sample.

3.3. Optical properties

The total reflection (TR) and the diffuse reflection (DR) rates versus the wavelength curves for the raw 304 SS substrate, Ag/304 SS substrate, 0.5-μm-thick Mo/304 SS substrate and 2-μm-thick Mo/304 SS substrate are shown in Fig. 8. The TR rate is defined as the ratio of the reflection light to the incident light. When the incident light angle is zero, any reflection light with an angle larger than 8° over the incident light is called the DR rate. The TR and DR rates are very important indexes for monitoring the light-trapping in thin-film solar cells. In general, high TR and DR rates indicate that the light path can be increased in the cell structure. Thus, scattered light within the absorbing layer increases the optical path length of the solar photons. The TR and DR rates of the Mo coating on the 304 SS substrate, whether being a 0.5-μm-thick or a 2-μm-thick Mo buffer layer were smaller than that of the raw 304 SS substrate. In addition, the TR and DR rates showed a slightly decreasing trend when the Mo buffer layer thickness increased from 0.5 μm to 2 μm. The cross-sectional SEM images in Figs. 7(c) and (d), show the roughened surface (large grain size and deep V-shaped trench) of the 2-μm-thick Mo buffer layer, which is believed to be the main reason for the low TR and DR rates of the thick Mo buffer layer. It was also found that the TR/DR rate at a

wavelength of 550 nm increased from 54.3%/7.7% of a raw 304 SS substrate to 84.2%/11.4% for the Ag coated 304 SS substrate. Previous work performed by our group showed that the surface texturing of different types of SS substrates after coating with Ag film revealed high TR and DR rates [13-14]. Coating an Ag film on the 304 SS substrate as a back reflector can help light absorption and further improve cell efficiency.
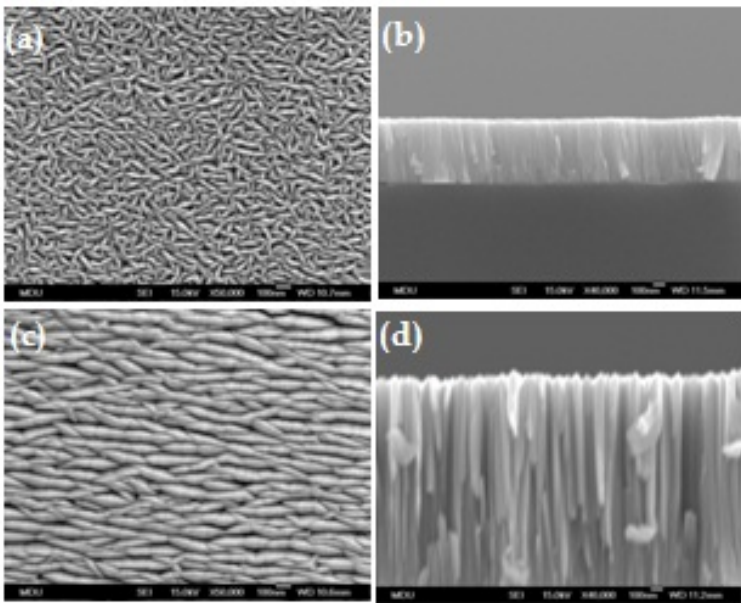

Figure 7. SEM images of the Mo buffer layer on a 304 SS substrate with a thickness of (a) 0.5-µm (b) 2-µm and cross sectional images of the Mo buffer layer with (c) 0.5-µm (d) 2-µm.
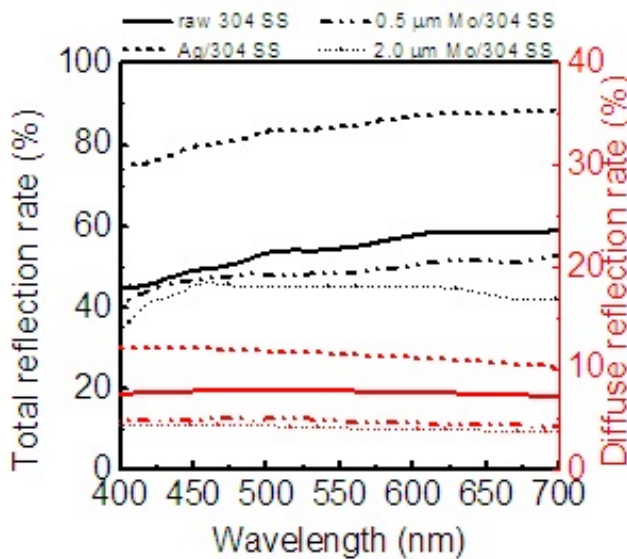

Figure 8. The TR and DR rates versus the wavelength curves of all the studied cells.

3.4. Current-voltage characteristics

Figure 9 shows the light J-V characteristics of all studied cells. The cell structure of Ag/AZO/n-i-p/Ag/SS has poor performances with $\eta=0.78\%$, FF = 29%, V_{oc} = 0.44 V and J_{sc} = 6.18 mA/cm^2. This poor cell efficiency may be due to several reasons, including incomplete absorption of incident light, and the presence of intrinsic or processing-induced defects. The light absorption of thin film solar cells can be enhanced by using the surface textured 304 SS substrate as a back-reflector. Since the DR and TR rates of the raw 304 SS substrate is low, a 200 nm thick Ag film was coated on the 304 SS substrate as a back-reflector. In Fig. 8, the increased TR and DR rates of the Ag coated 304 SS substrate was helpful for increasing the V_{oc} and J_{sc} of the a-Si:H thin film solar cell. However, the cell conversion efficiency of 1.3% is still too low for a-Si:H thin film solar cells, and the increased cell efficiency by using a metal Ag back-reflector is limited. On the other hand, the Fe impurities or iron-boron complex are deep-level defects in Si [23,24], and are known to have serious detrimental effects on the efficiency of crystalline Si solar cells. Thus, we suggest that these Fe impurities diffused from the 304 SS substrate into the a-Si:H thin film solar cells also form deep-level defects that deteriorates the cell's performance. A detailed and comprehensive understanding is necessary to address this process. In addition, a diffusion blocking layer is necessary to prevent the Fe impurities diffused from the 304 SS substrate to enter the a-Si:H thin film solar cells.
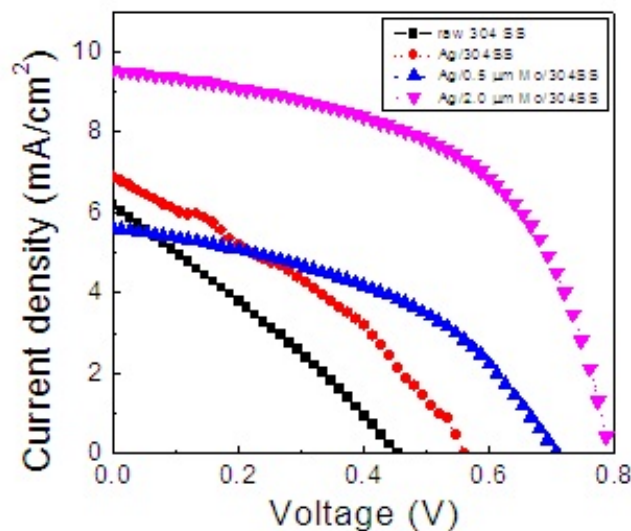

Figure 9. The J-V characteristics for all the studied cells.

3.5. Impurity diffusion in a-Si:H films

In order to study this Fe diffusion, we performed a SIMS analysis. Figure 10 shows the SIMS depth profile of the p-i-n a-Si:H thin film cells on the Ag/ 304 SS substrate and the Ag/2-μm-thick Mo/304 SS substrate. In Fig. 10(a), the Fe atom was detected in the whole p-i-n cell structure. In particular, the maximum signal intensity of the Fe atom was found at a depth of 500 nm in the Ag/AZO/n-i-p/Ag/SS substrate sample. The driving force of the Fe diffusion

from the 304 SS substrate into the p-i-n a-Si:H solar cells was believed to be due to the high temperature of the PECVD a-Si:H deposition process. The 200 nm Ag back-reflector can't prevent the Fe diffusion from the 304 SS substrate. In Fig. 10(b), the Fe atom signal intensity from the 304 SS substrate decreased with the increase in the thickness of the Mo buffer layer. In addition, almost no Fe atoms were detected in the p-i-n a-Si:H solar cells. It should be mentioned that few Fe atoms can diffuse through the 0.5-µm-thick Mo film into the a-Si:H layer. In Fig. 10(c), the cross-sectional SEM image indicates that the low sputtering rate of the Mo film has a dense columnar structure. High density, thin Mo films may be useful to suppress the diffusion of Fe atoms. However, we must consider the time-cost estimation. A 2-µm thick Mo film deposited at the low sputtering rate (0.28 nm/sec) requires 2 hrs, and at the high sputtering rate (1.11 nm/sec) it only requires 30 min. In addition, a 2-µm thick Mo film deposited at the high sputtering rate can effectively suppress the diffusion of Fe atoms into the a-Si:H layer. Thus, the optimal deposition condition for the Mo buffer layer is believed to be a thicker layer deposited at a high sputtering rate.
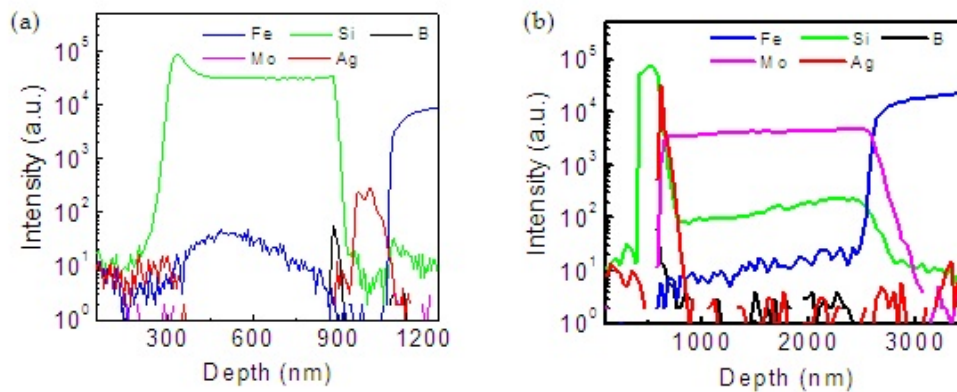

Figure 10. The SIMS depth profile of a-Si:H solar cells grown on (a) an Ag/304 SS substrate and (b) an Ag/2-µm Mo/304 SS substrate.

3.6. a-Si:H thin-film solar cells performance

Table 3 summarizes the relative cell performance of all studied cells. The best cell structure (i.e. Ag/AZO/n-i-p/Ag/2.0-µm-thick Mo/ SS) has a performance of η=4.12%, FF = 55%, V_{oc} = 0.78V and J_{sc} = 9.54 mA/cm^2. The R_{sh} was 119.1 Ω and 290.6 Ω for a-Si:H solar cell on the Ag coated 304 SS substrate and the Ag/2-µm-thick Mo film/304 SS substrate, respectively. In addition, the series resistance (R_s) of the Ag/AZO/n-i-p/Ag/ SS cell decreased from 53.3 Ω to 16.7 Ω for the Ag/AZO/n-i-p/Ag/2.0-µm-thick Mo/ SS cell. There are many reasons for the series resistance, including the resistance of the semiconductor bulk, contacts, interconnections, etc. Shunt resistance is believed to be caused mainly by lattice defects or leakage current at the edge of the solar cell. Based on the SIMS results, we believe that the high conversion efficiency was due to the effective prevention of the diffusion of Fe impurities. Fe impurities in the Si thin films will form deep-level defects that degenerate the junction interface in each layer of the cell structure thereby decreasing the R_{sh} of the solar cell. In addition, the Fe induced deep-level defects will increase the resistivity of the intrinsic a-Si:H layer which may raise the Rs. The high V_{oc} and J_{sc}

were due to an increase of Rsh and a decrease of Rs as a result of coating a thick Mo buffer layer on the 304 SS substrate. This effectively prevented Fe impurities from diffusing into the a-Si:H solar cells thereby improving the conversion efficiency of the solar cells. The improvement of the conversion efficiency of a-Si:H thin film solar cells on a 304 SS substrate by using a Mo buffer layer is still an open question. Some possible reasons might explain the improvement in cell efficiency by using a thick Mo buffer layer. For example, a thick Mo buffer layer decreases the surface roughness of the raw 304 SS substrate. The decrease in interface defect density of the a-Si:H thin-film solar cells due to the improved interface flatness results in an increased conversion efficiency as the Mo buffer layer thickness increases. However, we have to keep in mind that the thermal expansion coefficients of Si, Mo and stainless steel are 2.5×10^{-6}/K, 5.2×10^{-6}/K and 1.4×10^{-5}/K, respectively. Consequently, the a-Si:H layer grown directly on the stainless steel substrate will induce structural defects because of the severe mismatch in thermal expansion coefficients. The low thermal expansion coefficient of Mo film onto a stainless steel substrate can minimize the mismatch in thermal expansion coefficients between the a-Si:H layer and the 304 SS substrate. The density of the structural defects in the a-Si:H thin-film solar cells can be reduced, resulting in a high conversion efficiency of thin-film a-Si:H solar cells on the 304 SS substrate. More detailed experiments must be carried out in the future to allow us to understand the precise mechanism involved in improving cell efficiency by using a Mo buffer layer.

	V_{OC} (V)	J_{SC} (mA/cm^2)	P (mW)	FF (%)	η (%)	R_s (Ω)	R_{sh} (Ω)
Raw 304SS	0.44	6.18	0.78	29	0.78	58.1	82.5
Ag/304SS	0.54	6.88	1.3	35	1.3	53.3	119.1
Ag/0.5 μm Mo/ 304SS	0.7	5.6	1.75	44	1.75	49.1	286.3
Ag/2 μm Mo/ 304SS	0.78	9.54	4.12	55	4.12	16.7	290.6

Table 3. AM 1.5G output parameters of the a-Si:Hthin-film solar cells.

4. Surface treatment of the 304 stainless steel substrte to improve the conversion efficiency of a-Si:H solar cells

4.1. Experimental details

The a-Si:H thin-film solar cells were grown on 1-mm-thick 304 SS substrates by high-frequency plasma enhanced chemical vapor deposition (HF-PECVD) in an ultrahigh-vacuum, single-chamber, load-locked system at a constant temperature of 200 °C. The cell structures (see Fig. 11), consisting of Ag finger electrode/AZO/n-i-p/Ag/304 SS substrates were used to study the cells' performance on the EP and ECMP processed 304 SS substrate. The 60 nm Ag layer was deposited on the 304 SS substrate as a back reflector layer and back contact by radio frequency (RF) sputtering. The thickness of the n-i-p layers in the solar cell structure were 20, 300 and 10 nm, respectively. The 150-nm-thick AZO films were then grown on the

a-Si:H active layer by RF-sputtering. The EP process is an anodic dissolution of the surface polishing process. The 304 SS substrate was immersed in the electrolyte, and then a current of 4.5 A and voltage of 3.3 V was applied for 1 minute. For the ECMP process, the 304 SS substrate was treated with 3%wt $NaNO_3$ solution and 1 μm diameter alumina powders. The formation of the passivation layer on the 304 SS substrate during the initial ECMP process led to spikes on the sample surface that were readily removed by powder polishing. The ECMP process required roughly 5 minutes to achieve a mirror-like surface on the 304 SS substrate. The solar cell performance was measured using a calibrated AM 1.5G solar simulator under illumination, and operating at a light intensity of 100 mW/cm². The current density-voltage (J-V) curves were obtained using the Keithley 2400 Source Meter. The optical properties of the untreated 304 SS substrate and the EM/ECMP processed 304 SS substrate were measured by a UV-visible(Vis)-near IR (NIR) spectrophotometer (Perkin Elmer Lambda 750s) in the 300-1000 nm wavelength range. The samples were measured with a secondary ion mass spectroscope (SIMS) in order to analyze the diffusion of iron (Fe) and chromium (Cr) impurities from the 304 SS substrate into the cell structure.
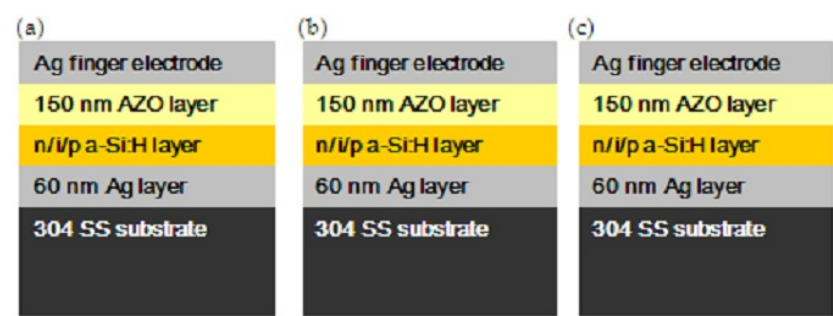

Figure 11. Cross-sectional schematic diagrams for the samples of this study.

4.2. Morphological properties

Fig. 12 shows the SEM and optical microscopy images of the untreated 304 SS substrate and the 304 SS substrate treated by EP and ECMP process. Fig. 12(a), shows many voids and scratches on the untreated 340 SS substrate surface. The surface roughness measured by 3D confocal microscopy, shows an average roughness (Ra) of ~ 330 nm for a surface area of 300×300 μm² for the untreated 304 SS substrate. Fig. 12(b), shows that the voids and scratches on the surface of the 304 SS substrate can be readily removed after the EP process. The smooth surface of the 304 SS substrate by means of the EP process was accomplished using the anode electrolysis mechanism that places the 304 SS substrate in the electrolyte and then applies the optimal voltage and current between the anode and the cathode electrode. In the 1980's, most of the research reports indicated that the EP process of the stainless steel substrate began by forming a viscous layer on the substrate surface resulting in the formation of a passivation layer. Generally, the high spike has a higher dissolve velocity in the viscous layer providing the initial polish of the stainless steel substrate. Once the EP process has ran for a long enough time, a dense passivation layer or metal-rich oxidation layer will form at

the bottom of the viscous layer on the surface of the substrate resulting in a smooth surface. However, the shortcoming of the EP process is that some small scratches and pin holes may remain that it cannot remove completely. Thus, this study used the ECMP process in an attempt to achieve a smoother surface of the 304 SS substrate. The ECMP process consists of both electrochemical and mechanical polishing mechanisms, electrolysis and physical polishing, to repair the irregular surface morphology of the 304 SS substrate. In addition, the mechanical friction between the polishing pad and the 304 SS substrate induces an interactive force that removes the surface oxidation layer or passivation layer that forms during the electrolysis process. It should be noted that no peeling force is generated during the ECMP process, and thus there is no need to consider any mechanical deformation of the substrate. Our experimental results indicated that the surface roughness of the 304 SS substrate can be reduced to 22 nm after having been treated by the ECMP process, as shown in Fig. 12(c).
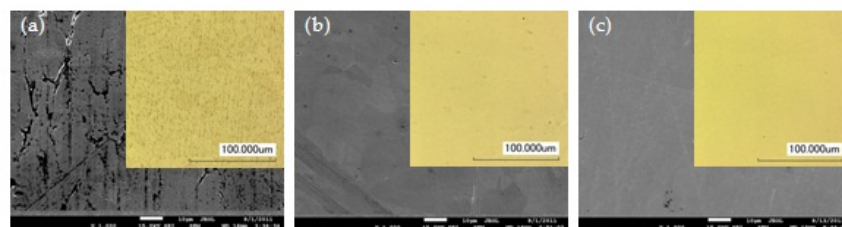

Figure 12. SEM and OM images of the (a) untreated 304 SS substrate, (b) EP, and (c) ECMP processed 304 SS substrate.

4.3. Optical properties

The effect of the surface morphology of the 304 SS substrate, treated by the EP and ECMP processes, on the light reflection properties were measured with a UV-visible-nIR spectrometer in the wavelength range of 300-1000 nm. As shown in Fig. 13, the average total reflection (TR) rate in the wavelength range of 300-1000 nm increased from 65.6 % for the untreated 304 SS substrate to 74.2 % and 73.7% respectively for the EP and ECMP processed 304 SS substrate. The average diffuse reflection (DR) rate was 3.8% for the untreated 304 SS substrate and decreased to 0.9% and 0.8% for the EP and ECMP processed 304 SS substrate, respectively. The high TR rate and low DR rate of the EP and ECMP processed 304 SS substrate were consistent with the SEM results. Thus, the EP and ECMP processes can achieve a smooth surface of the 304 SS substrate.

4.4. Current-voltage characteristics

Figure 14 shows the light current density and voltage (J-V) characteristics of all cells studied. The cell structure of the Ag finger electrode/AZO/n-i-p/Ag/untreated 304 SS substrate performed poorly with η=1.7 %, FF = 0.39, J_{sc} = 5.1 mA/cm^2, and V_{oc} = 0.79 V. Compared to the electrical properties of the a-Si:H thin-film solar cells grown on the glass substrate, the J_{sc} (i.e. ~ 15 mA/cm^2) is a key electrical property that needs to be improve in order to achieve a high con-

version efficiency of the a-Si:H thin-film solar cells on the 304 SS substrate. We first considered the incomplete absorption of incident light by the a-Si:H layer. It is known that the light absorption of thin-film solar cells can be enhanced by using a high reflectance metal as a back-reflector. Fig. 13 shows that the increased TR rate of the EP and ECMP processed 304 SS substrate was helpful to increase the J_{SC} of the a-Si:H thin-film solar cells. Compared with the a-Si:H thin-film solar cells on the untreated 304 SS substrate, the J_{sc} can be increased by about 35% and 43% for cells on EP and ECMP processed 304 SS substrates, respectively.
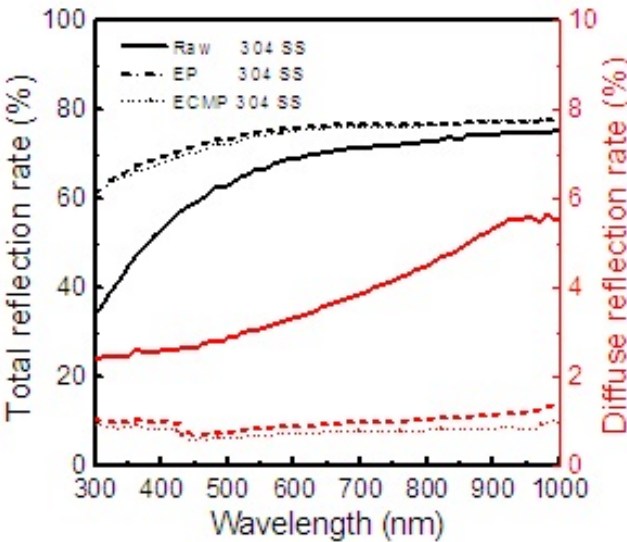

Figure 13. The TR and DR rates versus the wavelength curves of all the studied SS substrate samples.

It is worth noting that the difference of the average TR rates between the EP and ECMP processed 304 SS substrate was about 0.5%. However, the J_{sc} increased to 7.9 mA/cm² for cells on the EP processed 304 SS substrate, and to 9.0 mA/cm² for cells on the ECMP processed 304 SS substrate. Thus, another way to improve the J_{sc} of cells was associated with the intrinsic or processing-induced defects. In our previous study, we found that the Fe impurities that diffused from the 304 SS substrate into the a-Si:H layer deteriorated the cells' performance. The Fe impurities of the iron-boron complex are deep-level defects in Si, and are known to have serious detrimental effects on the efficiency of crystalline Si solar cells [25,26]. Thus, we believe that the impurities diffused from the 304 SS substrate into the a-Si:H thin-film solar cells form deep-level defects that deteriorate the cell's performance. A detailed and comprehensive understanding of the process is required to address this issue.

4.5. Impurity diffusion in a-Si:H films

In order to study the diffusion of impurities from the 304 SS substrate, we performed a SIMS depth profile analysis of the cell structure. Fig. 15 shows the SIMS depth profile of the p-i-n a-Si:H thin-film solar cells on the Ag/untreated 304 SS substrate, the Ag/EP processed 304 SS substrate and the Ag/ECMP processed 304 SS substrate. In Fig. 15(a), the Fe and Cr atoms

were detected in the whole p-i-n cell structure. The driving force of the Fe and Cr atoms diffusion from 304 SS substrate into the p-i-n a-Si:H solar cells was believed to be due to the high temperature of the PECVD a-Si:H layer deposition process. Fig. 15(b) shows that the intensity of the Fe and Cr atoms signals from the 304 SS substrate can be decreased by three orders of magnitude in the p-i-n a-Si:H layers. The dense Cr-rich passivation layer formed on the surface of the 304 SS substrate by the EP process is believed to act as a blocking layer to suppress the continual diffusion of Fe and Cr atoms from the 304 SS substrate during the high-temperature PECVD deposition process. The passivation layer can be a thin layer of oxidized metal that forms during the EP process. However, there remain some small scratches on the EP processed 304 SS substrate (see Fig. 12(b)) that provide the impurities diffusion with a channel into the a-Si:H layer. Thus, a small amount of Cr and Fe impurities can still diffuse into the a-Si:H layer. On the other hand, Fig. 15(c) shows that almost no Cr atoms are detected in the p-i-n a-Si:H layer. The ECMP process includes a mechanical polishing mechanism, and the mechanical friction between the polishing pad and the 304 SS substrate induces an interactive force that removes the Cr-rich passivation layer which formed during the electrolysis. Thus, we believe that the thickness of the Cr-rich passivation layer or oxidation layer on the ECMP processed 304 SS substrate is thinner than that of the EP processed 304 SS substrate. This thinner Cr-rich passivation layer may allow Fe atoms to diffuse into the a-Si:H layer. However, the dense and hard Cr-rich passivation layer on the 304 SS substrate which is generated during the electrolysis process will suppress the Cr atoms of the 304 SS substrate diffused into the a-Si:H layer.
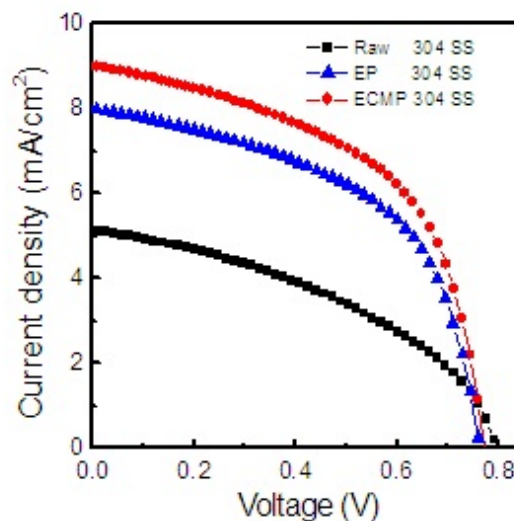

Figure 14. The J-V characteristics for all the studies cells.

4.6. a-Si:H thin-film solar cells performance

Table 4 summarizes the relative cell performance of all cells studied. The best cell for the a-Si:H grown on the ECMP processed 304 SS substrate had a performance of η =3.7 %, FF = 0.52, J_{sc} = 9.0 mA/cm^2, and V_{oc} = 0.78 V. The R_{sh} was 923 Ω and 1269 Ω for a-Si:H solar cells

grown on the untreated 304 SS substrate and ECMP processed 304 SS substrate, respectively. In addition, the series resistance (R_s) of the untreated 304 SS substrate cell decreased from 136 Ω to 72 Ω for the ECMP processed 304 SS substrate cell. There are many reasons for the series resistance, including the resistance of the semiconductor bulk, contacts, interconnections, etc. The shunt resistance is believed to be caused mainly by lattice defects or leakage current at the edge of the solar cell. Based on the SIMS results, we believe that the high conversion efficiency was due to the effective prevention of the diffusion of Cr and Fe impurities. The Cr and Fe impurities in the Si thin films form deep-level defects that degenerate the junction interface in each layer of the cell structure thereby decreasing the R_{sh} of the solar cell. In addition, the Cr and Fe induced deep-level defects increased the resistivity of the intrinsic a-Si:H layer which could increase the Rs. The high J_{sc} was due to an increase in R_{sh} and a decrease in R_s as a result of EP and ECMP processed 304 SS substrate. These processes effectively prevented Cr and Fe impurities from diffusing into the a-Si:H solar cells thereby improving the conversion efficiency of the solar cells.
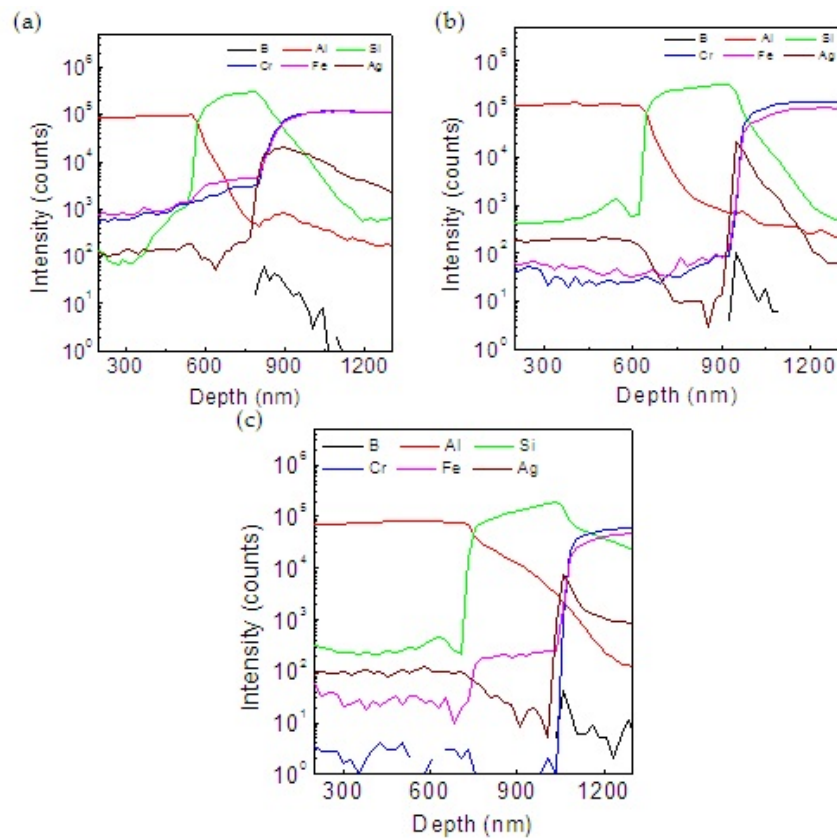

Figure 15. The SIMS depth profile of a-Si:H thin-film solar cells grown on (a) untreated 304 SS substrate, (b) EP and (c) ECMP processed 304 SS substrate.

In addition, the surface morphology and the diffusion of impurities into the 304 SS substrate influence the electrical performance of the a-Si:H thin-film solar cells. We must also keep in mind that the thermal expansion coefficients of Si, Ag and stainless steel are 2.5×10^{-6}/K, 1.95×10^{-5}/K and 1.4×10^{-5}/K, respectively. Consequently, the a-Si:H layer grown directly on the

Ag/stainless steel substrate will induce structural defects as a result of the severe mismatch in thermal expansion coefficients. In order to improve the thermal expansion mismatch issue, we inserted the ZnO:Al buffer layer between the a-Si:H layer and Ag/304 SS substrate. The thermal expansion coefficient of ZnO:Al is 5.3×10^{-6}/K. The low thermal expansion coefficient of ZnO:Al film onto a Ag/304 SS substrate can minimize the mismatch in thermal expansion coefficients between the a-Si:H layer and the 304 SS substrate. This reduces the density of the structural defects in the a-Si:H thin-film solar cells, resulting in a higher conversion efficiency of 4.5 % for a-Si:H thin-film solar cells on the ECMP processed 304 SS substrate. More detailed experiments including putting n-type a-Si:H down on the SS substrate side, adjusting the thickness of the ZnO:Al & Ag back-reflector must be carried out in the future to allow us to further improve cell efficiency.

	V_{oc} (V)	J_{sc} (mA/cm²)	FF (%)	η (%)	R_s (Ω)	R_{sh} (Ω)
Ag/Raw 304SS	0.79	5.1	39	1.7	136	923
Ag/EP 304SS	0.77	7.9	52	3.2	105	1286
Ag/ECMP 304SS	0.78	9.0	52	3.7	72	1269

Table 4. AM 1.5G output parameters of the a-Si:H thin-film solar cells.

5. Conclusions

This study presented the influence of the thickness of the metal Mo buffer layer on a 304 SS substrate on the performance of a-Si:H solar cells. The SIMS result showed that the Fe impurities can be blocked effectively by increasing the thickness of the Mo buffer layer to more than 2 μm. The increased V_{oc} and J_{sc} of a-Si:H solar cells on a Ag/Mo/304 SS substrate was due to an increased Rsh and a decreased R_s which related to the reduction of the Fe deep-level defects density. The Mo buffer layer functioning as an Fe impurities blocking layer plays an important role in improving the a-Si:H thin-film solar cells on a 304 SS substrate.

EP and ECMP surface treatment techniques were also used to smoothen the 304 SS substrate surface. A decreased surface roughness of untreated 304 SS substrate as a result of being subjected to the EP or ECMP process increased the TR rate. We believe that the high TR rate due to the smooth surface of the 304 SS substrate after undergoing the EP or ECMP process increased the short current density and as a result increased the cell conversion efficiency. In addition, the SIMS analysis indicated that the diffusion of Fe and Cr impurities from the 304 SS substrate into the a-Si:H solar cell can be suppressed by using the EP process. We suggested that due to the dense and hard Cr-rich passivation layer that was formed on the ECMP processed 304 SS substrate, the Cr impurity was nearly entirely prevented from diffusing into the a-Si:H layer, resulting in a decreased R_s and increase Rsh of the cell. The smooth surface and the low level of diffusion of impurities of the ECMP processed 304 SS

substrate play an important role in improving the conversion efficiency of the a-Si:H thin-film solar cells.

Acknowledgements

Author details

Wen-Cheng Ke and Shuo-Jen Lee

Department of Mechanical Engineering, Yuan Ze University, Chung-Li, 320, Taiwan, R.O.C.

References

[1] Hsu, . M., Tathireddy, P., Rieth, L., Normann, A. R., & Solzbacher, F. (2007). *Thin Solid Films 516 34.*

[2] Fan, Q. H., Chen, C., Liao, X., Xiang, X., Zhang, S., Ingler, W., Adiga, N., Hu, Z., Cao, X., Du, W., & Deng, X. M. (2010). *Sol. Energy Mater. Sol. Cells 94 1300.*

[3] Huran, J., Hotovy, I., Pezoltd, J., Balaykin, N. I., & Kobzev, A. P. (2006). *Thin Solid Films 515 651.*

[4] Deng, X. M., Liao, X. B., Han, S. J., Povolny, H., & Agarwal, P. (2000). *Sol. Energy Mater. Sol. Cells 62 89.*

[5] Kolodziej, A., Krewniak, P., & Nowak, S. (2003). *Opto-electronics Review, 11 281.*

[6] Ferlanto, A. S., Ferreira, G. M., Pearce, J. M., Wronski, C. R., Collins, R. W., Deng, X., & Ganguly, G. (2002). *J. Appl. Phys. 92 2424.*

[7] Zhou, D., & Biswas, R. (2008). *J. Appl. Phys. 103 093102.*

[8] Curtin, B., Biswas, R., & Dalal, V. (2009). *Appl. Phys. Lett. 95 231102.*

[9] Anna, J. A., Selvan, A. E., Delahoy, S., Guo, , & Li, Y. M. (2006). *Sol. Energy Mater. Sol. Cells, 90 3371.*

[10] Llopis, F., & Tobías, I. (2005). *Sol. Energy Mater. Sol. Cells, 87 481.*

[11] Sőderstrőm, T., Haug, F. J., Terrazzoni-Daudrix, V., & Ballif, C. (2008). *J. Appl. Phys. 103 114509.*

[12] Müller, J., Rech, B., Springer, J., & Vanecek, M. (2004). *Sol. Energy, 77 917.*

[13] Lee, S. J., Chen, S. L., Peng, C. W., Lin, C. Y., & Ke, W. C. (2007). *Mate. Chem. Phys. 118 219.*

[14] Lee, S. J., Lin, C. Y., Cheng, S. L., & Ke, W. C. (2011). *Mate. Chem. Phys. 130 733.*

[15] Reehal, H. S., Lesniak, M. P., & Hughes, A. E. (1996). *J. Phys. D: Appl. Phys. 29 934.*

[16] Ali, A., Gouveas, T., Hasan, M. A., Zaidi, S. H., & Asghar, M. (2011). *Sol. Energy Mater. Sol. Cells 95 2805.*

[17] Macdonald, D., Roth, T., Deenapanray, P. N. K., Bothe, K., Pohl, P., & Schmidt, J. (2005). *J. Appl. Phys. 98 083509.*

[18] Lim, S. Y., & Macdonald, D. (2007). *Sol. Energy Mater. Sol. Cells 95 2485.*

[19] Abbott, A. P., Capper, G., Mc Kenzie, K. J., & Ryder, K. S. (2006). *Electrochimica Acta. 51 4420.*

[20] Andrade, L. S., Xavier, S. C., Rocha-Filho, R. C., Bocchi, N., & Biaggio, S. R. (2005). *Electrochimica Acta. 50 2623.*

[21] Lin, C. C., & Hu, C. C. (2008). *Electrochimica Acta. 53 3356.*

[22] Hryniewicz, T. (1994). Surf. Coat Technol. 64 75

[23] Reehal, H. S., Lesniak, M. P., & Hughes, A. E. (1996). *J. Phys. D: Appl. Phys. 29 934.*

[24] Abdelbarey, D., Kveder, V., Schröter, W., & Seibt, M. (2010). *J. Appl. Phys. 108 043519.*

[25] Pickett, M. D., & Buonassisi, T. (2008). *J. Appl. Phys. 92 122103.*

[26] Macdonald, D., Roth, T., & Deenapanray, P. N. K. (2006). *Appl. Phys. Lett. 89 142107.*